Author Manuscript

Author Manuscript

Author Manuscript

Author Manuscript

HHS Public Access

Author manuscript

Stem Cells. Author manuscript; available in PMC 2017 June 20.

Published in final edited form as:

Stem Cells. 2015 August ; 33(8): 2537–2549. doi:10.1002/stem.2032.

Human iPSC-derived neural progenitors preserve vision in an AMD-like model

Yuchun Tsai[†], **Bin Lu**[†], **Benjamin Bakondi**, **Sergey Girman**, **Anais Sahabian**, **Dhruv Sareen**, **Clive N. Svendsen**, and **Shaomei Wang**[*]

Board of Governors Regenerative Medicine Institute, Department of Biomedical Sciences, Cedars-Sinai Medical Center, 8700 Beverly Boulevard, Los Angeles, CA 90048, USA

Abstract

Pluripotent stem cell derived retinal pigment epithelial (RPE) cells are currently being tested for cell replacement in late-stage age-related macular degeneration (AMD). However, preserving vision at early-stages may also be possible. Here we demonstrate that transplantation of neural progenitor cells (NPCs) derived from induced pluripotent stem cells (iNPCs) limits disease progression in the Royal College of Surgeons (RCS) rat, a preclinical model of AMD. Grafted-iNPCs survived, remained undifferentiated, and distributed extensively in a laminar fashion in the subretinal space. Retinal pathology resulting from the accumulation of undigested photoreceptor outer segments (POS) was significantly reduced in iNPC-injected rats compared with controls. Phagosomes within grafted-iNPCs contained POS, suggesting that iNPCs had compensated for defective POS phagocytosis by host-RPE. The iNPC-treated eyes contained 6–8 rows of photoreceptor nuclei that spanned up to 5 mm in length in transverse retinal sections, compared with only one row of photoreceptors in controls. iNPC treatment fully preserved visual acuity measured by optokinetic response. Electrophysiological recordings revealed that retina with the best iNPC-protected areas were 140-fold more sensitive to light stimulation than equivalent areas of contralateral eyes. The results described here support the therapeutic utility of iNPCs as autologous grafts for early-stage of AMD.

Correspondence should be addressed: Shaomei Wang, PhD, MD, 8700 Beverly Blvd., Cedars-Sinai Medical Center, Los Angeles, CA 90048, shaomei.wang@cshs.org.

[†]These authors contributed equally to this work.

The authors have declared that no conflict of interest exists

YT: Conception and design, collection and/or assembly of data, data analysis and interpretation, manuscript writing, final approval of manuscript.

BL: Conception and design, collection and/or assembly of data, data analysis and interpretation, manuscript writing, final approval of manuscript.

BB: Data analysis and interpretation, manuscript writing, final approval of manuscript.

SG: Collection and/or assembly of data, data analysis and interpretation.

AS: Provision of study material.

DS: Provision of study material.

CS: Provision of study material, manuscript editing and final approval of manuscript.

SW: Conception and design, data analysis and interpretation, financial support, manuscript writing, final approval of manuscript.

Author Manuscript Author Manuscript Author Manuscript Author Manuscript

Introduction

Retinal degenerative diseases, such as age-related macular degeneration (AMD) and retinitis pigmentosa (RP), are the major causes of irreversible blindness in industrialized countries (1–3). AMD pathogenesis involves a cascade of detrimental events beginning with RPE and Bruch's membrane changes that culminate in the death of light sensing photoreceptor cells and adjacent RPE ultimately leading to central vision loss. AMD is a multifactorial disease caused by the interaction of environmental factors, aging and genetic predisposition (2, 4), thus increasing the difficulty for rational drug design. Currently no effective treatment options exist to slow disease progression for dry AMD.

The use of stem/progenitor cells have shown tremendous promise for treating retinal degenerative diseases and three concurrent clinical trials for AMD are underway in the US (ClinicalTrials.gov). The clinical strategies for these trials are to use stem/progenitor cells to either replace the compromised host RPE, or to implant cells that limit ongoing RPE degeneration by undefined mechanisms. Our laboratory has performed numerous preclinical studies to evaluate the therapeutic potential of various stem and progenitor cell transplant strategies for retinal degenerative diseases, often using the RCS rat model in which cell treatments were evaluated for the aforementioned trials (5–7). RCS rats carry a mutation in the c-mer proto-oncogene tyrosine kinase (*Mertk*) gene that disrupts the ability of RPE cells to phagocytose the POS that is routinely shed during the diurnal visual cycle (8). The undigested POS accumulates as toxic debris in the subretinal space between the ONL and RPE, which blocks nutrient support of photoreceptors from the choroid vasculature, and results in progressive photoreceptor death and commensurate visual loss (9).

We have previously shown that subretinal injection of embryonic stem cell (ESC)-derived RPE cells as replacement significantly preserved vision in RCS rats (5, 6). However, evidence is lacking to show that grafted RPE cells had adopted the role of wild-type RPE cells *in vivo*, such as the phagocytosis of outer segments. In contrast, transplantation of human fetal central nervous system stem cells preserved vision in RCS rats and slowed retinal pathogenesis with an observed reduction in debris zone formation through the phagocytosis of outer segments (10). We also showed that subretinal injection of human cortical-derived NPCs ($hNPC^{ctx}$) dramatically rescued vision in the RCS rat (11, 12). Furthermore, $hNPC^{ctx}$ migrated long distances after subretinal injection, which would permit targeting of injections to parafovea of macula in patients to avoid further irrevocable central vision loss resulting from retinal detachment due to subretinal injection. $hNPC^{ctx}$ did not compromise normal retinal function after subretinal transplantation into non-human primates (13). In further support of safety for this treatment strategy, hNPCs did not form tumors following transplantation in the central nervous system of rodents or primates (14, 15), and have been used in several clinical trials (16) for neurological disorders with no adverse effects (17).

However, the clinical use of fetal-derived cells is complicated by ethical concerns, a limited and variable source of cells, as well as the potential for allograft immunogenicity. In contrast, iPSCs avoid these drawbacks and represent a promising cell source for future personalized therapies. iPSCs are derived from adult somatic cells using reprogramming

Author Manuscript Author Manuscript Author Manuscript Author Manuscript

factors and have the potential to become almost any cell type following exposure to specific culture conditions (18). We recently used human iPSCs to generate a stable neural progenitor cell line (iNPCs) that was similar to hNPC^{ctx} in morphology, ease of expansion, gene and protein expression profiles, as well as migration capacity and robust survival following transplantation (19). These iNPCs are multipotent and have significantly reduced tumorigenicity *in vivo* compared to iPSCs. The recent development of iNPCs now allows for limitless production of therapeutic cells for use in allogeneic and autologous transplantation.

In the current report, we show that subretinal injection of iNPCs into RCS rats preserved vision to a degree that is comparable with the other neuroprotective cell typed previously tested in our laboratory (5, 6, 12, 20). The extent of donor cell survival and distribution in the subretinal space, as well as photoreceptor and vision preservation were similar to that of hNPC^{ctx} under the same conditions in RCS rats (12). We observed that subretinal toxic debris accumulation was mitigated at graft sites via the iNPC-mediated phagocytosis of POS, which was associated with markedly slower degeneration and preserved visual function. Collectively, these data advocate for further development of iNPC grafts into translational therapies to treat retinal degeneration.

Materials and Methods

Animals and experimental designs

iNPCs were generated as described in detail previously (19). iPSC colonies were collected and suspended in Stemline Media (Sigma) supplemented with epidermal growth factor (EGF; 100 ng/ml; Millipore), fibroblast growth factor-2 (FGF-2; 100 ng/ml; Millipore), and heparin (5 μg/ml; Sigma). Fresh media was replaced after the first 2 days of sphere generation and subsequently every 3–4 days. The spheres were maintained in suspension, chopped every 7–10 days, and cryopreserved and thawed for cell banking.

Pigmented dystrophic RCS rats received unilateral subretinal injections of iNPCs (3×10^4/eye) at P21. The fellow eyes served as sham-operated or untreated controls. An intraperitoneal injection of dexamethasone was given for two weeks (1.6 mg/kg/day) after surgery. All animals were maintained on oral cyclosporine A, administered in the drinking water (210 mg/L). Animals were housed and maintained at the Cedars-Sinai Medical Center Department of Comparative Medicine vivarium. All animal protocols were approved by the Institutional Animal Care and Use Committee and all animals were treated in accordance with the ARVO Statement for the Use of Animals in Ophthalmic and Vision Research.

Transplantation

The iNPCs were not sorted prior to transplantation and included nestin (65%), glial fibrillary acidic protein (GFAP) (53%), S100β (74.5%) and TuJ1 (2.9%)-expressing cells, as detailed in our previous paper (19). iNPC neurospheres were dissociated by 10 minute (min) incubation with TrypLE (Life Technologies) and single cell suspensions generated by trituration with fire-polished glass Pasteur pipettes. Cells were then passed through a 30μm filter (Miltenyi Biotec, Auburn, CA, USA), washed twice with balanced salt solution (BSS, Alcon), gently triturated, and counted on a hemocytometer. Cell suspensions containing

Author Manuscript Author Manuscript Author Manuscript Author Manuscript

approximately 3×10^4 iNPCs in 2 μl BSS were kept on ice until transplantation. iNPCs were injected into the subretinal space according to our published protocol (6, 34). Briefly, a cell suspension containing 3×10^4 cells/eye in 2 μl of BSS carrying medium, was delivered into the subretinal space through a small scleral incision with a fine glass pipette (internal diameter, 75–150 μm) attached by tubing to a 25-μl syringe (Hamilton, Reno, NV). The cornea was punctured to reduce intraocular pressure and to limit the efflux of cells. A sham-surgery group was treated with BSS alone. Immediately after injection, the fundus was examined for retinal damage or signs of vascular distress. Any animals showing such problems were excluded from further study.

Visual function

All animals were tested by optokinetic response (OKR), Electroretinography (ERG) and luminance threshold recording (LTR) according to our published protocols (12, 34, 35). OKR offers non-invasive screening to detect visual acuity, but it is not a sensitive measurement to correlate photoreceptor thickness and visual acuity. ERG provides a gross measure of retinal activity and indicates the relative function of rods and cones; however, it is not sensitive enough to detect local subretinal effects. LTR from the superior colliculus measures the sensitivity to light stimuli across the visual field, which in turn provides a geographic indication of the magnitude and area of photoreceptor rescue across the retina.

Histology

Cryostat retinal sections were collected according to our previous protocol (34, 35). One slide from each set was stained with cresyl violet and remaining slides were stored at -40°C until used for immunostaining.

Quantification

ONL thickness and donor cell distribution were measured on cresyl violet-stained retinal sections (n=18) using Java-based image processing software version 1.46 (ImageJ; National Institutes of Health, Bethesda, MD).

Immunofluorescent staining and confocal microscopic imaging

Retinal sections were stained with the following antibodies with our published protocols (34,35) Cone-arrestin (rabbit polyclonal, 1:1,000; Millipore), PKCα (rabbit polyclonal, 1:5,000; Sigma), recoverin (rabbit polyclonal, 1:2,000; Millipore), calbindin D28k (rabbit polyclonal, 1:1,000; Swant), neurofilament-RT97 (mouse monoclonal, 1:1,000; Millipore), parvalbumin (rabbit polyclonal, 1:3,000; Swant), synaptophysin (mouse monoclonal, 1:2,000; Millipore), RPE65 (mouse monoclonal, 1:1,000; Millipore), type IV collagen (rabbit polyclonal, 1:1,000; Millipore), MAB1281 (mouse monoclonal, 1:300; Millipore), nestin (rabbit polyclonal, 1:2,000; Millipore), GFAP (rabbit polyclonal, 1:1,000; Sigma), S100β (mouse monoclonal, 1:250; Sigma), Ki67 (rabbit polyclonal, 1:500; Millipore), TuJ1 (mouse monoclonal, 1:1,000; Sigma), STEM121 (mouse monoclonal, 1:300; StemCells). Anti-mouse or rabbit secondary antibodies conjugated to Alexa Fluor-488 or Alexa Fluor-568 (Life Technologies) were used and counterstained with 49,69-diamidino-2-

Author Manuscript Author Manuscript Author Manuscript Author Manuscript

phenylindole (DAPI). Images were taken with a confocal microscope (Eclipse C1si; Nikon Instruments, Inc., Melville, NY).

Phagocytosis assays

Bovine photoreceptor outer segments (POS) were purchased (InVision BioResources, Cat# 98740) and labeled with fluorescein-5-isothiocyanate (FITC) (isomer I, Invitrogen) according to the manufacturer's instructions. iNPCs were fed with varying concentrations of POS (0.2, 1, and 2 μg/cm^2) for 15 min to 5 h at 37°C. Cells not fed POS were used as negative control to obtain baseline fluorescence. Cells were washed with PBS, followed by gently detaching cells and membrane bound POS by incubation with 0.05% trypsin for 5 min at 37°C. Stemline medium containing 2% fetal bovine serum (FBS) was added to neutralize the trypsin, followed by 4% paraformaldehyde fixation and DAPI counter staining. The number of iNPCs containing POS was determined by flow cytometry (LSR Fortessa analyzer, BD Biosciences). Data analysis was performed using FlowJo software. For POS degradation, iNPCs were fed 10 or 20 μg/cm^2 unlabeled POS for 3 h and followed by four rigorous PBS washes to remove non-binded POS. iNPCs were collected at 6, 15, 24, and 48 h post-POS feeding and harvested for Western blot analysis to determine the time course of rhodopsin degradation.

Western blot analysis

Cells were lysed in RIPA buffer containing PMSF and protease inhibitor cocktail (Cat# sc-24948, Santa Cruz) for 30 min on ice and centrifuged for 15 min at 13,000 rpm. Protein concentrations were determined by bicinchoninic acid protein assay kit (Pierce) according to the manufacturer's instructions. Protein lysates were denatured by adding 2 × laemmli buffer (Cat# 161-0737, Bio-Rad) containing 5% β-mercaptoethanol (Sigma). Protein samples (10 to 30 μg) were separated on 7.5% or 10% sodium dodecyl sulfate-polyacrylamide gels and transferred onto polyvinylidene difluoride (PVDF) membranes (Millipore). Membranes were blocked in 5% nonfat dry milk in Tris buffered saline plus 0.1% Tween-20 and incubated with primary antibodies overnight at 4°C, followed by 3 PBS washes and incubation with horseradish peroxidase-conjugated secondary antibodies (1:3,000, Santa Cruz) for 1 h at RT. Detection of the immunoreactive bands was performed with the ECL Western Blotting Substrate (Pierce), and chemiluminescence was detected with the Bio-Rad imaging system. PVDF membranes were stripped with glycine buffer plus 0.1% β-mercaptoethanol and re-probed with the appropriate antibodies. Primary antibodies raised against the following proteins were used for western blots: rhodopsin (mouse monoclonal, 1:500; Millipore), Mertk (monoclonal, 1:1,000; abcam), and β-actin (monoclonal, 1:5,000; Sigma).

RT-PCR analysis

Total mRNA was extracted (RNeasy mini kit, Qiagen) and genomic contamination removed (DNase I, Life Technologies). cDNA was synthesized using 1 μg of total RNA (High Capacity RNA-to cDNA kit, Applied Biosystems) and PCR was performed using gene-specific primers (table 1) and Taq DNA Polymerase (Thermo Scientific) according to the manufacturer's instructions. No template controls (NTC) contained all reagents but lacked

Author Manuscript Author Manuscript Author Manuscript Author Manuscript

RNA template, and genomic controls lacked inclusion of reverse transcriptase (RT controls). PCR products were analyzed by on 2% agarose gel electrophoresis.

Transmission electron microscopy

Retinal whole mount was prepared according to our published protocol (10). Retinas were processed for immunohistochemistry with primary antibody, STEM121 and incubated with biotinylated secondary IgG antibody (Vector Laboratories, Inc., Burlingame, CA), followed by avidin-biotin complex staining (ABC kit; Vector Laboratories, Inc.) and reaction with 3,38-diaminobenzidine tetrahydrocholoride (Vector Laboratories, Inc.). Retinal area with positive stain was dissected and mounted in the sandwich. After dehydration and embedding in Epon, semi-thin and thin sections were cut, counter stained with uranyl acetate and lead citrate. The grids were viewed and photographed under a JEM-1011 electron microscope (JEOL Ltd).

Statistical Analysis

Group sample sizes were determined in order to achieve 95% power to detect a significant difference between treated and control groups. Visual acuity and *b*-wave amplitudes of iNPC-treated, sham-treated, or untreated eyes ($n = 12–15$ rats per group) were analyzed by one-way ANOVA with Bonferroni post-hoc power analyses (GraphPad Prism 5 statistical analysis software). P values ≤ 0.05 were considered significant. An unpaired, two-tailed Student's t-test was used to determine the significance of responses from the superior colliculus (SC)of iNPC-treated and untreated eyes ($n = 4$ per group). Error bars indicate standard error mean (SEM). Asterisks and # signs indicate significance, $*P \leq 0.05$, $**P \leq 0.01$, $***P \leq 0.001$.

Results

Subretinal iNPC transplants preserved visual function

iPSCs were derived from control human fibroblasts as previously described in detail (19). Graft survival and visual function were assessed in animals that received iNPCs, BSS (sham), or were left untreated at P60, P90 and P150. Spatial visual acuity in units of cycle/degree (c/d) assessed by optokinetic response (OKR) was significantly higher in iNPC-treated rats compared with sham-treated and untreated controls at all-time points (Fig. 1A, P60: 0.53±0.024/c/d vs. 0.48±0.007c/d and 0.45±0.027c/d, both $P < 0.001$; P90: 0.54±0.24c/d vs. 0.32±0.04c/d and 0.31±0.04c/d, both $P < 0.001$; P150: 0.54±0.02c/d vs. 0.25±0.04c/d, and 0.25±0.04c/d, both $P < 0.001$). Visual acuity decreased between P60 and P150 in untreated ($P < 0.001$) and sham-treated ($P < 0.001$) RCS rats, while OKRs showed sustained visual acuity in iNPC-injected eyes between the same time-points ($P = 0.72$).

In addition, retinal electrical responses to light stimulation were measured by electroretinography (ERG). *A*-wave amplitudes were low (4–8 μV) in iNPC-treated animals at P60 and were undetectable in control rats, suggesting that rod function was severely compromised in all experimental groups. In contrast, *b*-wave amplitudes following iNPC transplantation were significantly higher when compared to those of sham-treated eyes (Fig. 1B, P60: 107.56±22.94 μV vs. 24.29±10.63 μV, $P < 0.001$; P90: 82.17±23.73 μV vs.

Author Manuscript Author Manuscript Author Manuscript Author Manuscript

4.41±1.45 μV, $P < 0.001$; P150: 42.1±10 μV vs. 6.07±2.19 μV, $P = 0.037$) and untreated eyes (Fig. 1B, P60: 8.75±4.1 μV, $P < 0.001$; P90: 4.4±1.45 μV, $P < 0.001$; P150: 6.13±2.66 μV, $P = 0.038$). ERG *b*-wave amplitudes decreased over the time points tested in iNPC-injected eyes (P60–P90, $P = 0.019$; P90–P150, $P = 0.005$), indicating that retinal degeneration was slowed, but not stopped by cell treatment.

Finally, detailed maps of retinal sensitivity to light stimulation were generated by recording luminance threshold responses (LTR) from contralateral superior colliculi (SC) (12, 21). The SC area that responded to luminance of 0.65 log units, which we defined as “hot spots”, was not statistically different in the iNPC transplant group between P90 (40%) and P150 (42.22%) ($P = 0.80$, Fig. 1C). However, luminance of 1.6 log units elicited responses from iNPC-treated eyes that corresponded to 90% and 58% of the total measureable SC area at P90 and P150, respectively, whereas identical light stimulation of untreated eyes did not produce responses (Fig. 1C). The rate of vision loss was dramatically slowed by iNPC treatment.

Visual tests compared the function of treated and untreated (contralateral) eyes from individual rats, which served as an internal control for variation between animals. Data for OKR, ERG, and LTR at P150 are shown (Fig. 1D–F). OKR: treated vs. untreated, 0.511c/d vs. 0.233c/d (Fig. 1D). ERG: 52.63 μV vs. 3.97 μV (Fig. 1E). LTR: 1.8±1.09 vs. 2.9±0.36 log units (Fig. 1F). The hot spot in the SC of the iNPC-injected retina was 140-fold more sensitive than the equivalent area in the contralateral eye ($P < 0.001$). A clear difference between iNPC-treated and contralateral untreated eyes was observed in all functional tests.

Subretinal iNPC transplants preserved photoreceptors, inner retina synapses, and RPE morphology

To test whether iNPC grafts preserved photoreceptors, frozen retinal transverse sections were stained with cresyl violet from rats that received iNPC transplants, BSS (sham), or were untreated. A marked protection of photoreceptors in iNPC-treated eyes was observed at P90 with an ONL thickness of 8 nuclei (Fig. 2A) and at P150 with an ONL thickness of 3–6 nuclei (Fig. 2D) in comparison to sham-treated (P90: Fig. 2B; P150: Fig. 2E) and untreated eyes (P90: Fig. 2C; P150: Fig. 2F). This was in contrast to the ONL with just one discontinuous row of photoreceptors in sham (P90: Fig. 2B; P150: Fig. 2E) and untreated eyes (P90: Fig. 2C; P150: Fig. 2F). Within an individual animal, the ONL at P150 was 3–6 nuclei thick in the iNPC-treated eye (Fig. 2G, upper) compared to a single discontinuous layer of ONL in the fellow eye (Fig. 2G, lower). Rescued photoreceptors were exclusively observed in areas juxtaposed to iNPC grafts at P90 (Fig. 2A) and P150 (Fig. 2D). Quantification of ONL length with 3 or more nuclei in thickness correlated with the length of the parallel iNPC graft at P150 (Fig. 2H: 3,353±717μm vs. 3,221±920μm; $P = 0.39$; $r^2 = 0.6937$).

Photoreceptor preservation was characterized by immunostaining for cone arrestin in iNPC-treated retinas, which showed normal cone morphology with pedicles, axons, as well as inner and outer segments (Fig. 3A), while typical cone morphology was absent in sham-treated retinas at P90 (Fig. 3B). Recoverin immunostaining also showed that iNPC-treated eyes had morphologically preserved photoreceptors with fully formed inner segments (Fig.

Author Manuscript Author Manuscript Author Manuscript Author Manuscript

3C), compared with that of sham-treated retinas (Fig. 3D). Immunostaining for the secondary retinal neurons showed that rod bipolar cells (revealed by protein kinase C, PKCα) had greater axon terminal density in iNPC-grafted eyes compared with that of controls (Fig. 3C and 3D). The dendrites and axons of horizontal cells (cell body and dendrites revealed by calbindin D28k, axons by neurofilament-RT97) were well preserved with denser dendrites and organized axons in graft areas compared with controls (Fig. 3E and 3F).

Furthermore, immunostaining of the presynaptic marker, synaptophysin, in iNPC-grafted retinas revealed a contiguous thick layer in the OPL and greater coverage in the IPL (Fig. 3G) compared with that of sham-treated eyes (Fig. 3H). A cobblestone-like RPE morphology (anti-RPE65, green, Fig. 3I) and an organized basement membrane (Collagen-IV, red, Fig. 3K) were observed in iNPC-graft areas, while hypertrophic RPE (Fig. 3J) with a disorganized basement membrane were evident at sites distal from the graft, (Fig. 3L).

Transplanted iNPCs displayed extensive survival, distribution, and maintained progenitor cell phenotype

We characterized the survival, distribution, and differentiation of the grafted iNPCs, as these factors may influence the preservation of photoreceptors and visual function. Immunostaining for human-specific nestin and human nuclear marker MAB1281 showed that iNPCs survived up to 130 days in RCS retinas, and that the majority had migrated between the RPE and photoreceptor layers, with only few cells observed in the inner retina (Fig. 4A). Additional immunostaining revealed that iNPCs expressed neural progenitor and glial markers nestin, S100β, and GFAP as previously described (19) (Fig. 4A–C), and failed to express differentiation markers of RPE cells (RPE65), neurons (TuJ-1), or retinal neurons (recoverin or PKCα; data not shown). These data suggest that grafted-iNPCs largely remained as phenotypically uncommitted progenitor cells throughout the study.

The iNPCs were consistently observed within a layer of graft-derived extracellular matrix, which was demonstrated by human-specific antibody staining (ongoing study). In addition, measurements from frozen retinal sections demonstrated that grafts had broadly distributed, with a maximum length of 5,034 μm at P90, and 4,300 μm at P150. While grafts had robust survival and demonstrated broad distribution, we found no evidence of teratoma formation up to and including the P150 time-point in any animal (Fig. 2G, upper). Regardless, tumorigenicity remains a concern with the use of iPSC-derived cells, and we therefore stained iNPC-grafted retinas for the co-expression of the cell proliferation marker, ki67, with the human nuclear marker, MAB1281 (Fig. 4D). We very infrequent found double-positive cells, which were only observed as individual cells, as opposed to a proliferative mass of cells.

Grafted-iNPCs preserved vision through POS phagocytosis and degradation

The deleterious *Mertk* mutation in RCS rats obstructs normal phagocytosis in RPE cells (8), which results in the accumulation of undigested POS, termed *debris zones* (DZ), which ultimately compromise vision. While NPCs from fetal or iPSC sources can improve vision for many months in the RCS rat, their mechanism of action remains unclear. To this end, we

Author Manuscript Author Manuscript Author Manuscript Author Manuscript

observed that the DZ was drastically reduced in iNPC-protected areas compared to areas distant from the grafts (Fig. 3C, 3D), suggesting that the grafted-iNPCs restored POS phagocytosis to RCS rats. We first assessed whether the iNPCs expressed the genes typically related with POS phagocytosis found in RPE cells. Using RT-PCR, we confirmed that iNPC expression of mRNA transcripts associated with POS binding (*Itgav and Intb5*), internalization and degradation (*Ctsd, Clt-a, Fak*), and POS-specific internalization (*Mertk*), was similar to that of human fetal RPE which was used as a positive control (Fig. 5A). Western blot analysis further confirmed Mertk protein expression (Fig. 5B). Given that the iNPCs expressed genes relevant for phaocytosis, we next tested the ability of iNPCs to phagocytose POS *in vitro*. iNPCs were seeded onto chamber slides, grown to 70% confluence, and exposed to FITC-conjugated bovine POS for 5 hours (h) followed by immunolabelling with human cytoplasmic marker STEM121 (Fig. 5C). Three-dimensional cross-section analysis of confocal images showed FITC-labeled POS within the cytoplasm of iNPCs (Fig. 5C′). The rate and extent of phagocytosis by iNPCs was next examined using a flow cytometry-based assay. Confluent iNPC cultures were given FITC-conjugated POS for 5 h and subsequently labeled with nuclear marker DAPI to distinguish cells from isolated POS. The percent of iNPCs that phagocytosed POS was determined and normalized to the background fluorescence of non-POS-exposed iNPCs in the FITC channel. The data showed that 18.7% of the iNPCs phagocytosed POS at 0.2 μg/cm^2 and the percentage of FITC-POS-containing iNPCs increased in a linear relationship with additional FITC-POS concentrations (Fig. 5D). To monitor the dynamics of POS phagocytosis in iNPCs, 0.2 μg/cm^2, 1.0 μg/cm^2 and 5.0 μg/cm^2 FITC-conjugated POS was incubated with iNPCs for 15 minutes (m), 30 m, 2 h, and 5 h. Median fluorescence intensity (MFI), represented the amount of POS ingested and showed that the percent of POS-containing iNPCs was proportional to MFI at various POS concentrations and time-points, with the highest MFI achieved with 5 μg/cm^2 POS at 5 h. Given the high percentage of iNPCs that phagocytosed POS (90%, Fig. 5E), we next evaluated the capability of iNPCs to degrade the ingested POS. iNPCs were exposed to rhodopsin-containing POS (10 μg/cm^2 or 20 μg/cm^2) for 3 h and analyzed via Western blot at 6, 15, 24, and 48 h time-points to determine the degradation rate of rhodopsin (Fig. 5G). In the absence of POS, no rhodopsin was detected in iNPC cultures. Rhodopsin was undetectable in iNPCs by 24 h post incubation with 10 μg/cm^2 POS, and by 48 h post feeding with 20 μg/cm^2 POS (Fig. 5G). Similar results were reported in iPSC-derived RPE cells (23).

Having confirmed that iNPCs can phagocytose and degrade POS *in vitro*, we next examined whether grafted-iNPCs contained phagosomes *in vivo* by electronic microscopy (EM). Retinal whole mounts were prepared from iNPC- and sham-treated eyes at P60 and immunostained with STEM121 (dark peroxidase staining) to visualize donor cells (Fig. 6A, B). Semi-thin and thin retinal sections were analyzed by EM. In iNPC-treated eyes, STEM121-positive donor cells (Fig. 6A, arrowheads) were detected along with rescued photoreceptors (ONL), organized inner segments (IS), and outer segments (OS). The ONL of sham-treated eyes was reduced in thickness to 3–4 nuclei with a typical DZ (Fig. 6B). Furthermore, typical DZ was prominent in a sham-treated retina (Fig. 6B), which was greatly reduced in the iNPC-grafted retina (Fig. 6A). At higher magnification, different stages of digested POS were seen close to the grafted cells (Fig. 6C, D) and engulfed

Author Manuscript Author Manuscript Author Manuscript Author Manuscript

membranous discs were visible inside the cytoplasm of iNPCs (Fig. 6E, F, human STEM121 positive staining). Collectively, these data demonstrate that grafted-iNPCs preserved retinal structure and visual function in RCS rats, at least in part by compensating for the defect in host-RPE to phagocytose and degrade POS.

Discussion

In the current study, we show that visual function was dramatically preserved at 2 and 4 months following unilateral subretinal injection of iNPCs preceding photoreceptor degeneration in RCS rats. Within the subretinal space, iNPCs persisted and self-assembled into a discrete stratified sheet of cells that encompassed part of the diseased retina where we observed normal retinal lamination, RPE morphology, and retinal synapse density in areas parallel to grafted cells. Morphologically preserved areas of RPE and ONL corresponded to enhanced electrophysiological responses to light stimulation in contralateral superior colliculi, suggesting that retinal physiology in grafted areas was maintained at P90 and P150. By OKR, visual acuity was preserved up to 150 days. Similarly, ERG recordings at P90 and P150 time-points showed substantial preservation with iNPC treatment compared with that of controls. Grafted-iNPCs lacked expression for markers of differentiated cells, yet expressed genes required for POS phagocytosis and contained RPE-like pigmented granules. Further analysis of electron micrographs established that transplanted iNPCs compensated for the Mertk deficiency in RCS rats by ingesting and clearing shed POS, which otherwise accumulated into toxic debris that instigated photoreceptor apoptosis in control retinas. This is the first description of a mechanism of action for how transplanted iNPCs preserve visual function in a pre-clinical model of AMD.

The rationale for transplanting terminally differentiated RPE cells to replace RPE lost to AMD spurred several pre-clinical studies in RCS rats in which significant vision rescue was achieved. Donor RPE cells for the clinical trials were derived from ESCs (ACT, Inc.), iPSCs (Riken Institute), or HuCNS-SC (Stem Cells, Inc.) and vision improvement was recently reported in the phase I safety study using ESC-RPEs. Ten of 18 AMD or Stargardt's macular dystrophy patients experienced vision improvement 22 months following transplant, despite presenting with end-stage central vision loss at the time of enrollment (24). Optimism from these safety data led to a phase II trial, with approximately 100 patients set to start in early 2015.

The strategy of using RPE transplants in the form of cell sheets, however, may be selectively applicable for treating late-stage AMD, as pre-atrophic host RPE and underlying choroid vasculature would be separated by grafts that may prevent sufficient nutrient support of photoreceptors. The already hostile environment of the diseased retina poses additional obstacles for achieving successful vision rescue. For example, RPE-sheets previously placed in central atrophic areas showed poor survival and led to the altered strategy of targeting *transient zones* adjacent to atrophic areas. RPE-sheet migration following transplant, however, was reported to be poor (25) and requisite engraftment onto the existing Bruch's membrane may be prevented from AMD-associated calcification and reduction of local ECM components, such as collagen, elastin, and laminin. Furthermore, apical-basal polarity may need to be re-established by donor RPE for proper epithelial homeostasis. To this end,

Author Manuscript Author Manuscript Author Manuscript Author Manuscript

RPE-sheets grown on scaffolds with pre-established polarity showed greater retinal survival and function following transplant (26–28), however, artificial implants risk further reducing the ONL nutrient supply and may elicit immunogenicity.

The surgical invasiveness of RPE-sheet implantation poses further risk to vision loss from retinal detachment, potentially limiting this treatment to patients with severely compromised RPE to warrant the procedure. The use of RPE in the form of cell suspensions obviates the need for targeted placement as cells can migrate to the atrophic macula with reduced surgical risk and may provide a better option for late-stage dry AMD. However, the time by which RPE dysfunction has progressed to advanced stages with significant enough cell loss to support RPE replacement, the level of concomitant ONL degeneration may necessitate the co-transplantation of photoreceptors. Grafted RPE cells may need to integrate onto the existing Bruch's membrane and photoreceptors may need to traverse the hypertophic outer limiting membrane to form synapses with bipolar and horizontal neurons, and the *de novo* synaptogenesis required for photoreceptor replacement has been described as an inefficient process (29, 30).

More generally, the fact that multiple factors emanating from tissues other than the RPE have been linked to AMD etiology questions the rationale and possibility for success of RPE replacement. Genetic and environmental factors of atrophic AMD predispose patients to immune-related and oxidative stresses that compromise RPE function concurrently with photoreceptor loss (31). In addition, defects originating in Bruch's membrane, such as increased hydrophobicity, reduced permeability, and impaired nutrient exchange between the choroid and the RPE, have also been suggested to play a causative role in AMD (32). Therefore, early intervention is the optimal approach for maximal rescue of retinal anatomy and vision. Here we show that grafted-iNPCs preserved existing retinal function without direct cell replacement, and thus without the complex requirements of grafts that are intended for tissue replacement, such as host tissue integration or organotypic polarization. Rather, the lack of iNPC differentiation and host-tissue integration may serve as an advantage, as grafted cells cohered as an auxiliary sheet distinct from host retinal tissue, yet dramatically slowed retinal degeneration flanking the graft site. Furthermore, iNPCs self-assembled as layer of graft-derived extracellular matrix that did not require attachment to Bruch's membrane to support long-term retinal function. These data suggest that iNPCs are suited for treating AMD with multifactorial disease etiology, and particularly well-suited for early intervention that is prior to substantial cell loss, for which cell replacement therapy is likely premature.

A previous study showed that subretinal injection of $hNPC^{ctx}$ preserved both photoreceptors and long-term visual function (11, 12), and POS phagocytosis was observed in stem cells from a similar source after grafting into RCS rats (10). However, clinical application of fetal-derived cells is limited due to ethical concerns, having a variable cell source, as well as the potential for allograft immunogenicity. The use of iNPCs averts each of these issues. However, a potential shortcoming we observed with our iNPC transplants was that the *b*-wave amplitudes by ERG decreased between P90 and P150, and this change correlated with a decrease in size of ONL-protected areas, suggesting that degeneration was slowed rather than halted. This limitation of stem cell therapies has also been reported in studies that used

Author Manuscript Author Manuscript Author Manuscript Author Manuscript

different stem cell treatment paradigms (6, 12, 25). In our current study, central hot spots in the SC representative of preserved retina did not change position over time, but rather diminished in coverage. Decreases in size of ONL-preserved areas proceeded radially inward from the leading edge toward areas opposite to the graft center (Fig. 2C). The slight decrease in iNPC graft coverage at the peripheral edge may have been due to the progressive retinal vascular leakage that is characteristic to aged RCS rats (22). Pathological vascular changes initiate at non-grafted areas, and may later encroach into iNPC-protected areas. Consequently, the immune-privileged nature of the eye can become compromised and iNPC xenografts might be targeted for clearance (33). Despite cyclosporine-mediated immunosuppression via the drinking water, immunogenicity remains possible as we previously showed that systemically delivered cyclosporine may be below effective levels of immunosuppression (7). Immune-mediated graft clearance is best circumvented with the use of autologous grafts that are non-immunogenic, such as with the iNPCs described here.

To address translational implications, we must consider that the major concern of AMD patients is the safe and long-term preservation of central vision. A single subretinal injection of iNPCs into the RCS rats at the early stage of degeneration preserved photoreceptors and vision to 130 days post-transplantation. When normalized to the average lifespan for their species, 130 days of preserved vision in rats roughly equates to 16 years in humans. In addition, the translational significance of long-distance iNPC migration is that it allows injections to be targeted to parafovea of macula to avoid further surgical risk to the already compromised fovea of AMD patients. It is remains critical to further investigate whether injection of iNPCs at the later stage of degeneration would still be effective as this may be more clinically relevant. Importantly, while immune rejection of allografts in humans remains to be explored, iNPCs could be used in an autologous fashion if required. We conclude that iNPCs hold real promise to preserve existing retinal structure and vision during the early-stages of AMD.

Acknowledgments

This work was supported by The Simon and Beatrice Apple Stem Cell Fund for Eye Research, David and Janet Polak Foundation Stem Cell Core Laboratory; NIH (R01 EY020488), Department of Defense (W81XWH-12-1-0617), Foundation Fighting Blindness, Board of Governors Regenerative Medicine Institute at Cedars-Sinai Medical Center, Knights Templar Eye Foundation, Inc (YT).

We thank Dr. Soshana Svendsen and Ms. Melissa K. Jones for review and editing, Dr. Gouping Fan for providing human fetal RPE cells, Dr. Alberto Yáñez for assistance with flow cytometry, and the Cedars-Sinai Medical Center Microscopy Core for assistance with electron microscopy.

References

1. Klein R. Overview of progress in the epidemiology of age-related macular degeneration. Ophthalmic Epidemiol. 2007; 14:184–187. [PubMed: 17896295]
2. Lim LS, Mitchell P, Seddon JM, Holz FG, Wong TY. Age-related macular degeneration. Lancet. 2012; 379:1728–1738. [PubMed: 22559899]
3. Ratnapriya R, Chew EY. Age-related macular degeneration-clinical review and genetics update. Clin Genet. 2013; 84:160–166. [PubMed: 23713713]
4. Anasagasti A, Irigoyen C, Barandika O, López de Munain A, Ruiz-Ederra J. Current mutation discovery approaches in Retinitis Pigmentosa. Vision Res. 2012; 75:117–129. [PubMed: 23022136]

Author Manuscript Author Manuscript Author Manuscript Author Manuscript

5. Lund RD, Wang S, Klimanskaya I, Holmes T, Ramos-Kelsey R, Lu B, Girman S, Bischoff N, Sauvé Y, Lanza R. Human embryonic stem cell-derived cells rescue visual function in dystrophic RCS rats. Cloning Stem Cells. 2006; 8:189–199. [PubMed: 17009895]
6. Lu B, Malcuit C, Wang S, Girman S, Francis P, Lemieux L, Lanza R, Lund R. Long-term safety and function of RPE from human embryonic stem cells in preclinical models of macular degeneration. Stem Cells. 2009; 27:2126–2135. [PubMed: 19521979]
7. McGill TJ, Cottam B, Lu B, Wang S, Girman S, Tian C, Huhn SL, Lund RD, Capela A. Transplantation of human central nervous system stem cells - neuroprotection in retinal degeneration. Eur J Neurosci. 2012; 35:468–477. [PubMed: 22277045]
8. D'Cruz PM, Yasumura D, Weir J, Matthes MT, Abderrahim H, LaVail MM, Vollrath D. Mutation of the receptor tyrosine kinase gene Mertk in the retinal dystrophic RCS rat. Hum Mol Genet. 2000; 9:645–651. [PubMed: 10699188]
9. Mullen RJ, LaVail MM. Inherited retinal dystrophy: primary defect in pigment epithelium determined with experimental rat chimeras. Science. 1976; 192:799–801. [PubMed: 1265483]
10. Cuenca N, Fernández-Sánchez L, McGill TJ, Lu B, Wang S, Lund R, Huhn S, Capela A. Phagocytosis of photoreceptor outer segments by transplanted human neural stem cells as a neuroprotective mechanism in retinal degeneration. Invest Ophthalmol Vis Sci. 2013; 54:6745–6756. [PubMed: 24045996]
11. Wang S, Girman S, Lu B, Bischoff N, Holmes T, Shearer R, Wright LS, Svendsen CN, Gamm DM, Lund RD. Long-term vision rescue by human neural progenitors in a rat model of photoreceptor degeneration. Invest Ophthalmol Vis Sci. 2008; 49:3201–3206. [PubMed: 18579765]
12. Gamm DM, Wang S, Lu B, Girman S, Holmes T, Bischoff N, Shearer RL, Sauvé Y, Capowski E, Svendsen CN, Lund RD. Protection of visual functions by human neural progenitors in a rat model of retinal disease. PLoS One. 2007; 2:e338. [PubMed: 17396165]
13. Francis PJ, Wang S, Zhang Y, Brown A, Hwang T, McFarland TJ, Jeffrey BG, Lu B, Wright L, Appukuttan B, Wilson DJ, Stout JT, Neuringer M, Gamm DM, Lund RD. Subretinal transplantation of forebrain progenitor cells in nonhuman primates: survival and intact retinal function. Invest Ophthalmol Vis Sci. 2009; 50:3425–3431. [PubMed: 19234356]
14. Behrstock S, Ebert A, McHugh J, Vosberg S, Moore J, Schneider B, Capowski E, Hei D, Kordower J, Aebischer P, Svendsen CN. Human neural progenitors deliver glial cell line-derived neurotrophic factor to parkinsonian rodents and aged primates. Gene Ther. 2006; 13:379–388. [PubMed: 16355116]
15. Emborg ME, Ebert AD, Moirano J, Peng S, Suzuki M, Capowski E, Joers V, Roitberg BZ, Aebischer P, Svendsen CN. GDNF-secreting human neural progenitor cells increase tyrosine hydroxylase and VMAT2 expression in MPTP-treated cynomolgus monkeys. Cell Transplant. 2008; 17:383–395. [PubMed: 18522241]
16. Glass JD, Boulis NM, Johe K, Rutkove SB, Federici T, Polak M, Kelly C, Feldman EL. Lumbar intraspinal injection of neural stem cells in patients with amyotrophic lateral sclerosis: results of a phase I trial in 12 patients. Stem Cells. 2012; 30:1144–1151. [PubMed: 22415942]
17. Robberecht W, Philips T. The changing scene of amyotrophic lateral sclerosis. Nat Rev Neurosci. 2013; 14:248–264. [PubMed: 23463272]
18. Yamanaka S. Induced pluripotent stem cells: past, present, and future. Cell Stem Cell. 2012; 10:678–684. [PubMed: 22704507]
19. Sareen D, Gowing G, Sahabian A, Staggenborg K, Paradis R, Avalos P, Latter J, Ornelas L, Garcia L, Svendsen CN. Human induced pluripotent stem cells are a novel source of neural progenitor cells (iNPCs) that migrate and integrate in the rodent spinal cord. J Comp Neurol. 2014
20. Wang S, Lu B, Wood P, Lund RD. Grafting of ARPE-19 and Schwann cells to the subretinal space in RCS rats. Invest Ophthalmol Vis Sci. 2005; 46:2552–2560. [PubMed: 15980247]
21. Girman SV, Wang S, Lund RD. Time course of deterioration of rod and cone function in RCS rat and the effects of subretinal cell grafting: a light- and dark-adaptation study. Vision Res. 2005; 45:343–354. [PubMed: 15607350]
22. Wang S, Lu B, Lund RD. Morphological changes in the Royal College of Surgeons rat retina during photoreceptor degeneration and after cell-based therapy. J Comp Neurol. 2005; 491:400–417. [PubMed: 16175546]

Author Manuscript Author Manuscript Author Manuscript Author Manuscript

23. Singh R, Shen W, Kuai D, Martin JM, Guo X, Smith MA, Perez ET, Phillips MJ, Simonett JM, Wallace KA, Verhoeven AD, Capowski EE, Zhang X, Yin Y, Halbach PJ, Fishman GA, Wright LS, Pattnaik BR, Gamm DM. iPS cell modeling of Best disease: insights into the pathophysiology of an inherited macular degeneration. Hum Mol Genet. 2013; 22:593–607. [PubMed: 23139242]
24. Schwartz SD, Regillo CD, Lam BL, Eliott D, Rosenfeld PJ, Gregori NZ, Hubschman J-P, Davis JL, Heilwell G, Spirn M, Maguire J, Gay R, Bateman J, Ostrick RM, Morris D, Vincent M, Anglade E, Del Priore LV, Lanza R. Human embryonic stem cell-derived retinal pigment epithelium in patients with age-related macular degeneration and Stargardt's macular dystrophy: follow-upof two open-label phase 1/2 studies. Lancet. 2014:1–8.
25. Carr AJ, Vugler AA, Hikita ST, Lawrence JM, Gias C, Chen LL, Buchholz DE, Ahmado A, Semo M, Smart MJ, Hasan S, da Cruz L, Johnson LV, Clegg DO, Coffey PJ. Protective effects of human iPS-derived retinal pigment epithelium cell transplantation in the retinal dystrophic rat. PLoS One. 2009; 4:e8152. [PubMed: 19997644]
26. Lee CJ, Fishman HA, Bent SF. Spatial cues for the enhancement of retinal pigment epithelial cell function in potential transplants. Biomaterials. 2007; 28:2192–2201. [PubMed: 17267030]
27. Bhatt NS, Newsome DA, Fenech T, Hessburg TP, Diamond JG, Miceli MV, Kratz KE, Oliver PD. Experimental transplantation of human retinal pigment epithelial cells on collagen substrates. Am J Ophthalmol. 1994; 117:214–221. [PubMed: 8116750]
28. Stanzel BV, Liu Z, Somboonthanakij S, Wongsawad W, Brinken R, Eter N, Corneo B, Holz FG, Temple S, Stern JH, Blenkinsop TA. Human RPE Stem Cells Grown into Polarized RPE Monolayers on a Polyester Matrix Are Maintained after Grafting into Rabbit Subretinal Space. Stem Cell Reports. 2014; 2:64–77. [PubMed: 24511471]
29. Eberle D, Kurth T, Santos-Ferreira T, Wilson J, Corbeil D, Ader M. Outer segment formation of transplanted photoreceptor precursor cells. PLoS One. 2012; 7:e46305. [PubMed: 23029471]
30. Gonzalez-Cordero A, West EL, Pearson RA, Duran Y, Carvalho LS, Chu CJ, Naeem A, Blackford SJ, Georgiadis A, Lakowski J, Hubank M, Smith AJ, Bainbridge JW, Sowden JC, Ali RR. Photoreceptor precursors derived from three-dimensional embryonic stem cell cultures integrate and mature within adult degenerate retina. Nat Biotechnol. 2013; 31:741–747. [PubMed: 23873086]
31. Barnett BP, Handa JT. Retinal microenvironment imbalance in dry age-related macular degeneration: a mini-review. Gerontology. 2013; 59:297–306. [PubMed: 23406680]
32. Sohn, RFMaEH. Age Related Macular Degeneration - The Recent Advances in Basic Research and Clinical Care. 2012; chap. 3:50–72.
33. Streilein JW, Ma N, Wenkel H, Ng TF, Zamiri P. Immunobiology and privilege of neuronal retina and pigment epithelium transplants. Vision Res. 2002; 42:487–495. [PubMed: 11853765]
34. Lu B, Morgans CW, Girman S, Luo J, Zhao J, Du H, Lim S, Ding S, Svendsen C, Zhang K, Wang S. Neural Stem Cells Derived by Small Molecules Preserve Vision. Translational Vision Science & Technology. 2013; 2:1.
35. Wang S, Lu B, Girman S, Duan J, McFarland T, Zhang QS, Grompe M, Adamus G, Appukuttan B, Lund R. Non-invasive stem cell therapy in a rat model for retinal degeneration and vascular pathology. PLoS One. 2010; 5:e9200. [PubMed: 20169166]

Author Manuscript Author Manuscript Author Manuscript Author Manuscript

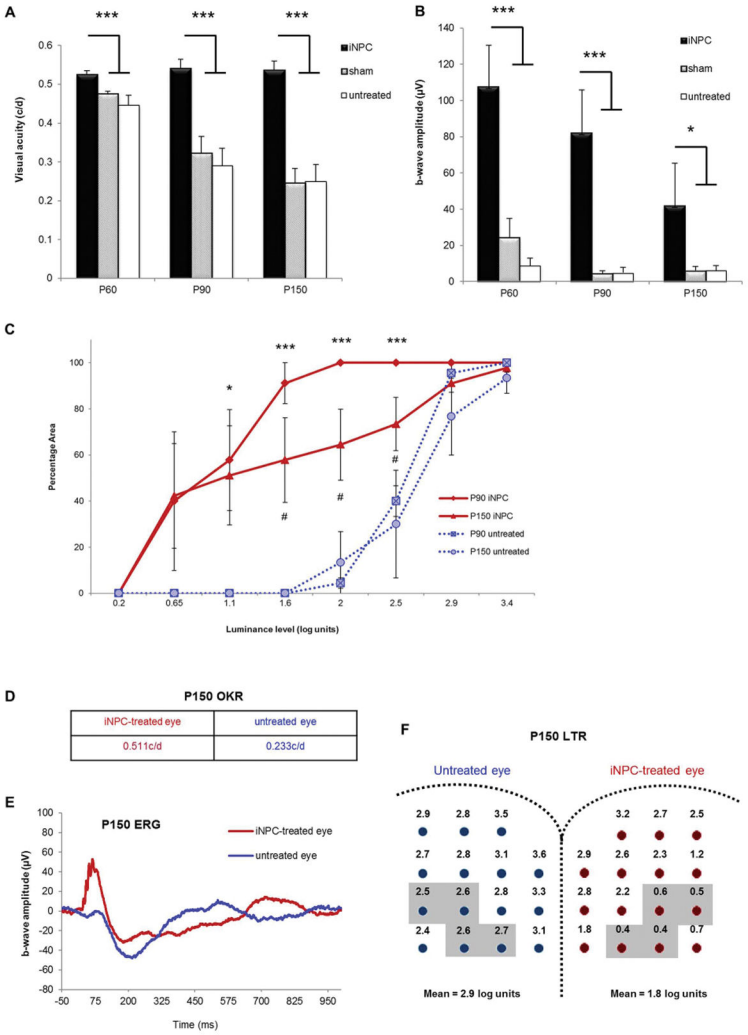

Fig. 1. iNPC transplants preserved visual function

(**A–D**) RCS rats at P21 received a subretinal injection of 3×10^4 iNPCs or BSS or were left untreated. (**A**) Spatial visual acuity determined by OKR was significantly greater in iNPC-treated eyes compared with controls at P60, P90, and P150 (n = 12–15 rats/group). (**B**) Photopic ERGs showed that cone *b*-wave amplitudes were higher in iNPC-treated eyes compared with controls (n = 12–15 rats/group). (**C**) Luminance threshold recording (LTR) showed that in iNPC-treated eyes, 90% and 58% of the SC area responded to light stimulation of 1.6 log units at P90 (n = 4 per group) and P150 (n = 4 per group), respectively. In contrast, no response was detected in untreated eyes at the same time points. (D–F) P150 data from a representative animal exemplifies the differences observed between iNPC-treated and contralateral (untreated) eyes. (**D**) OKR from one animal showed that the iNPC-treated eye had markedly higher acuity than the contralateral untreated eye (0.511c/d vs. 0.233c/d). (**E**) ERG showed that the *b*-wave amplitude was greater in the iNPC-treated compared with the untreated eye. (**F**) LTR from 15 sites representing approximately 80% of the SC surface area showed that the iNPC-treated eye had consistently greater light-sensitivity than the fellow eye at P150 (1.8 vs. 2.9 log units). The hot spots were highlighted.

Author Manuscript Author Manuscript Author Manuscript Author Manuscript

All graphs display mean ± SEM, and statistical significance was determined by one-way ANOVA (A, B) and paired, two-tailed Student's *t* tests (C) (*$P \leq 0.05$; ***$P \leq 0.001$; #$P \leq 0.05$).

Author Manuscript Author Manuscript Author Manuscript Author Manuscript

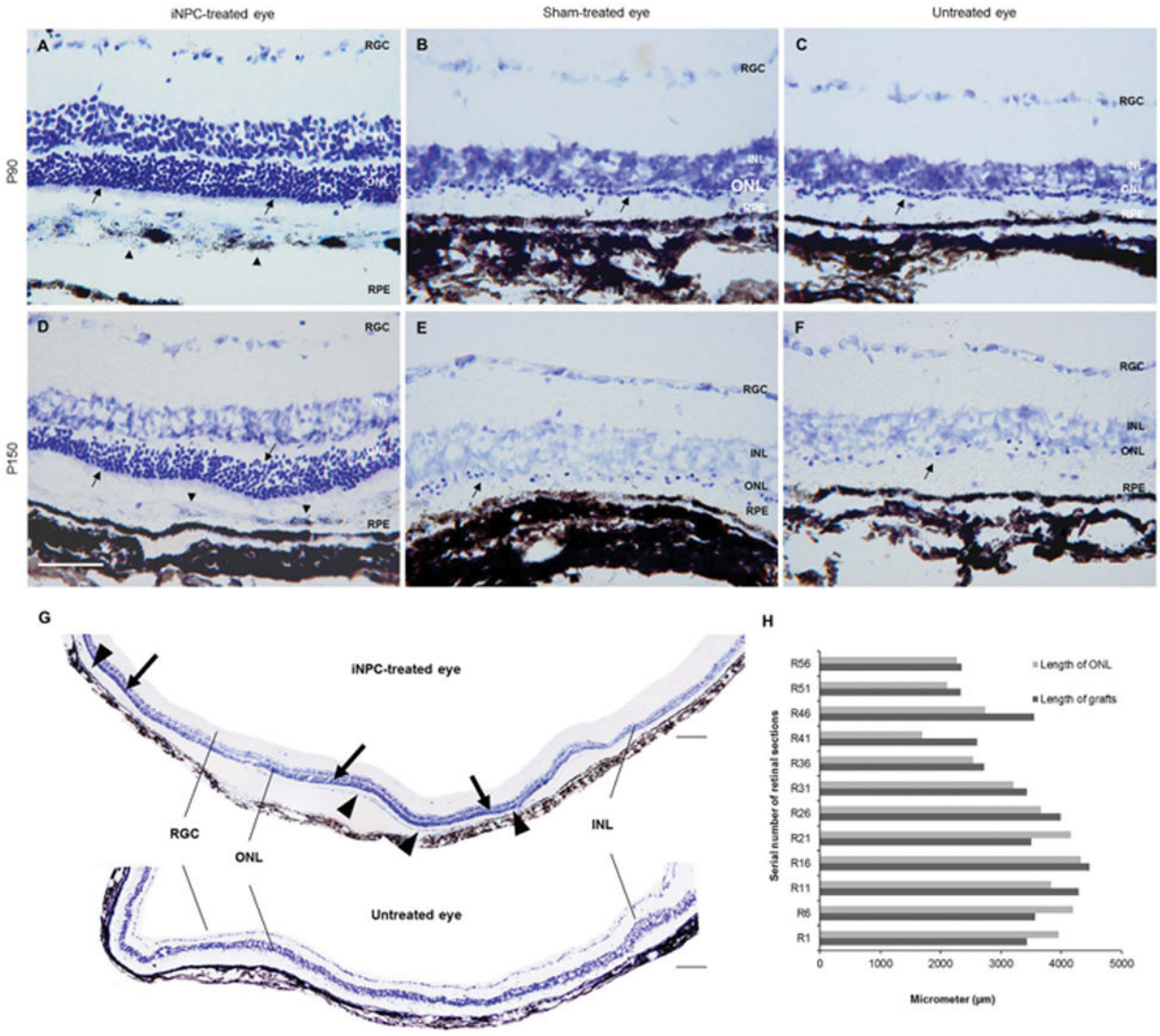

Fig. 2. iNPC transplants preserved photoreceptors

Cresyl violet (CV) stained retinal sections showed marked preservation of outer nuclear layer (ONL) in iNPC-treated eyes at P90 (**A**) and P150 (**D**), while sham-treated (**B, E**) and untreated eyes (**C, F**), had only one layer of photoreceptor cells (black arrows). An extra layer of cells containing pigment granules was frequently observed as a discontinuous sheet with a depth of 1–3 cell nuclei residing between the RPE and ONL in iNPC-treated eyes (A and D, arrowheads). Scale bars: 50 μm. (**G**) Tile-scanned images of CV stained retinal sections at P150 from iNPC-treated (upper) and untreated eye (lower) showed that the number of photoreceptors had largely remained in the iNPC-treated (arrows) versus untreated eye (3–6 layers vs. 1 discontinuous layer of photoreceptors). Grafted iNPCs formed a layer and contained melanosome-like pigment granules (arrowheads). Scale bars: 100 μm. (**H**) Graph shows that the length of preserved ONL (defined as three or more nuclei in thickness) correlated with the length of iNPC-grafted area ($P > 0.05$). Statistical

Author Manuscript Author Manuscript Author Manuscript Author Manuscript

significance was determined by paired, two-tailed Student's *t* test. RGC: retinal ganglion cells; INL: inner nuclear layer; ONL: outer nuclear layer; RPE: retinal pigment epithelium.

Author Manuscript Author Manuscript Author Manuscript Author Manuscript

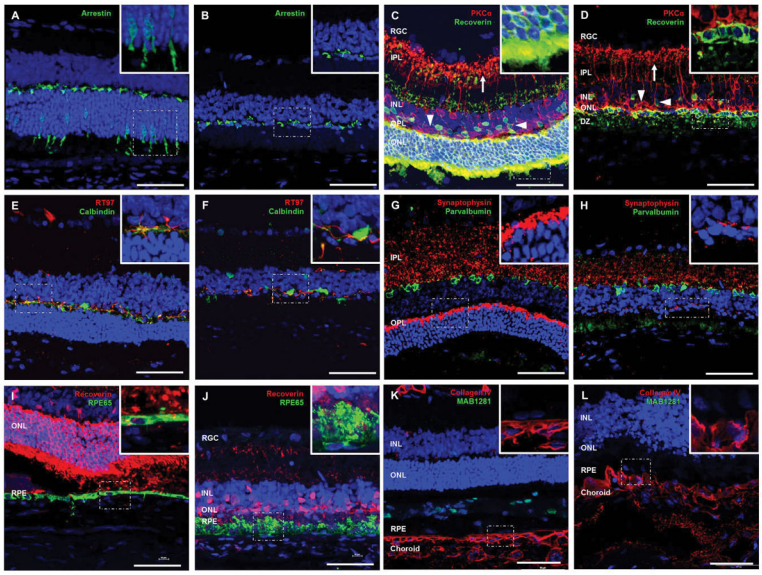

Fig. 3. iNPCs preserved photoreceptors, synaptic connections, and RPE morphology

Confocal images of P90 RCS rat retinas that received iNPCs (**A, C, E, G**) or BSS (**B, D, F, H)** at P21 are shown. (**A, B**) Cone photoreceptor (by arrestin antibody) was preserved in iNPC-treated (**A**) compared with sham-treated eyes (**B**). (**C, D**) Retinal sections immunostained for recoverin (green), PKCα (red), and DAPI (blue) showed obvious ONL rescue in iNPC- (**C**) versus BSS-treated eyes (**D**). Axon terminals of bipolar cells (red) were substantially reduced in BSS-treated (**D**) compared with iNPC-treated retinas (**C**). Cone bipolar cells (green) are shown (**C, D**, left arrowheads) with reduced synaptic terminal density in the IPL of BSS-treated retinas (**D**, arrow). (**E, F**) Horizontal cell bodies (anti-calbindin D28k, green) and axons (anti-RT97, red) showed greater co-localization (yellow) in iNPC-treated eyes (**E**) compared with controls (**F**). (**G, H**) Presynaptic terminals in the IPL (anti-synaptophysin; red) were consistently denser with iNPC (**G**) versus BSS (**H**) treatment. AII amacrine cells (anti-parvalbumin; green) showed no difference between treatments. (**I**) RPE (anti-RPE65, green) in areas juxtaposed to preserved ONL (anti-recoverin, red) had contiguous morphology, while in area away from the grafts, hypotrophic RPE was evidence (**J**). The basement membrane of RPE (anti-collagen-IV, red) in areas juxtaposed to grafted cells (anti-MAB1281, green) showed organized structure (K), compared with disorganized basement membrane in area away from the grafts (L). Insets show enlarged images corresponding to boxed regions. RGC: retinal ganglion cells; IPL: inner plexiform layer; INL: inner nuclear layer; OPL: outer plexiform layer; ONL: outer nuclear layer; RPE: retinal pigment epithelium; DZ: debris zone. Scale bars: 50 μm.

Author Manuscript Author Manuscript Author Manuscript Author Manuscript

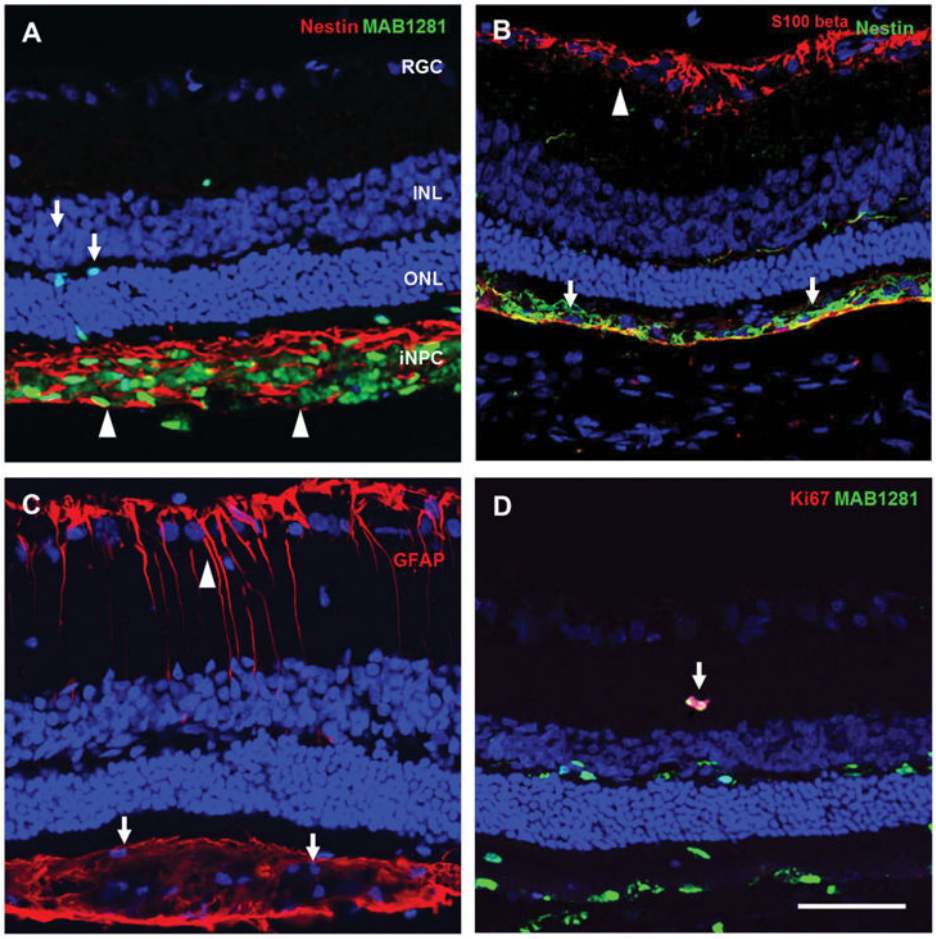

Fig. 4. Transplanted iNPCs broadly distributed and maintained an uncommitted phenotype

(**A**) The identity of iNPCs was determined by immunolabeling for human nuclei (MAB1281, green) and human-specific nestin (red). At P90, donor cells had distributed in the subretinal space and were observed as a uniform sheet of approximately 2–3 cell nuclei in thickness (up arrowheads). Donor cells were only sporadically observed in the inner retina (down arrows). Grafted iNPCs expressed the glial markers S100β (**B**) and GFAP (**C**) shown by down arrows. S100β and GFAP were expressed by retinal astrocytes (**B** & **C,** arrowheads). (**D**) Only one donor cell was observed double-positive for the proliferative marker, Ki67 (red), and MAB1281 (green). RGC: retinal ganglion cell; INL: inner nuclear layer; ONL: outer nuclear layer; RPE: retinal pigment epithelium; iNPC: iPSC-derived neural progenitor cell. Scale bars: 50 μm.

Author Manuscript Author Manuscript Author Manuscript Author Manuscript

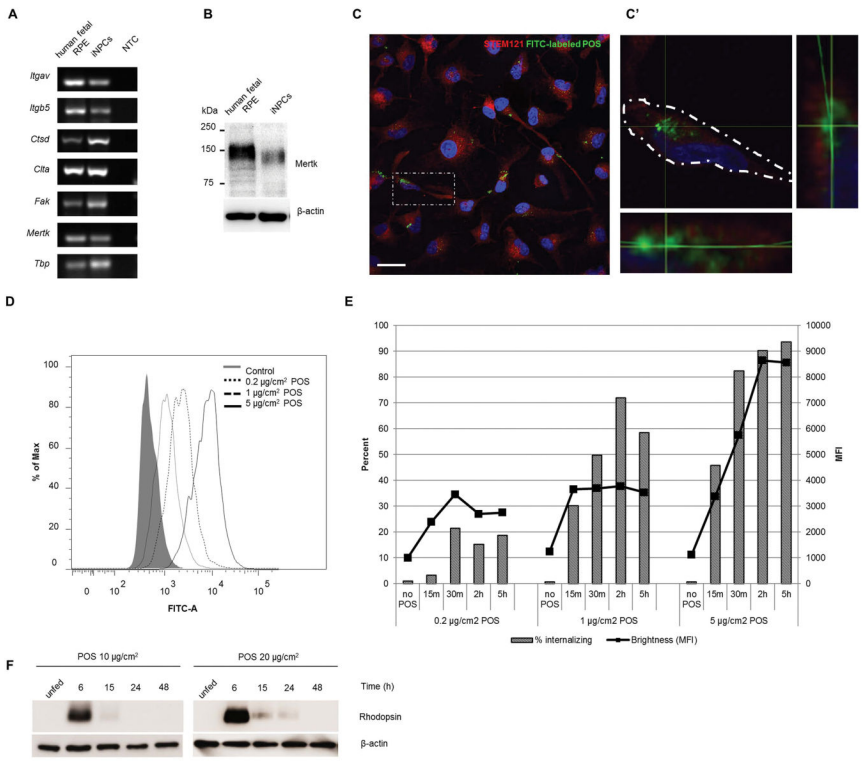

Fig. 5. iNPCs expressed genes required for POS phagocytosis, phagocytosed and degraded POS *in vitro*

(**A**) mRNA transcripts required for POS phagocytosis were detected in iNPCs and human fetal RPE cells by RT-PCR. The housekeeping gene, *Tbp,* served as the endogenous control, and no bands were observed in the no-mRNA template control (NTC) lane. (**B**) The protein expression of Mertk was confirmed by Western blot. β-actin was used as endogenous control. (**C**) Z-stack fluorescence confocal microscopy images of STEM121-stained iNPCs (red) show internalized FITC-labeled POS (green). DAPI was used as counterstain nuclei (blue). (**C′**) Enlargement of the image outlined by the dashed box in C shows a single confocal optical slice in which Z-axes depth is indicated by the green lines. Scale bar: 50 μm. (**D**) iNPCs were fed 0.2, 1, and 5 μg/cm^2 FITC-labeled POS for 5 h and the flow cytometric quantification (histogram) showed that iNPCs internalized POS in a dose-dependent manner. (**E**) The percent of cells internalizing FITC-labeled POS (left: y-axis) and MFI (right: x-axis) represented the amount of POS phagocytosed by iNPCs. (**F**) Western blot analysis showed that rhodopsin content in iNPCs at 6 h was degraded at 24 or 48 h following the initial 3h POS feeding with either 10 or 20 μg/cm^2 unlabeled POS, respectively.

Author Manuscript Author Manuscript Author Manuscript Author Manuscript

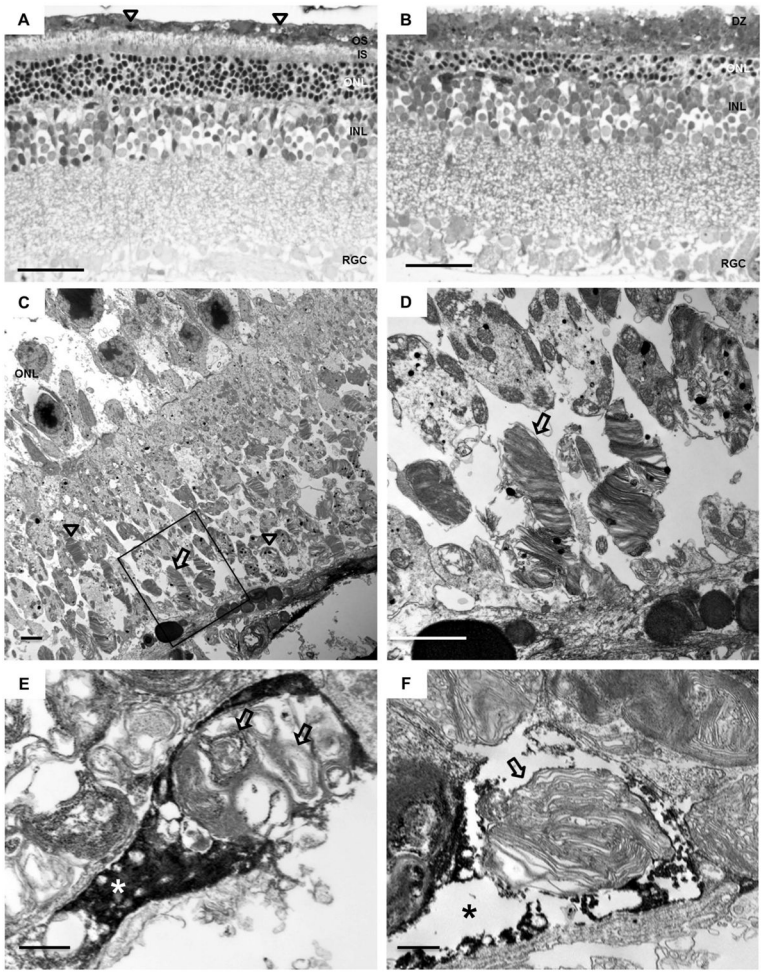

Fig. 6. iNPCs phagocytosed POS *in vivo*

Semi-thin sections from whole mount retinas across the iNPC-graft area (**A**) or from sham-treated eyes (**B**) at P60 were stained with 1% Toluidine blue. (**A**) A layer of contiguous donor cells stained with human specific-marker STEM121 was observed (arrowheads). Adjacent to the iNPC graft, the ONL, IS, and OS structures were preserved. (**C**) OS at various stages of digestion were found beneath ONL (arrows). High magnification EM image of the outlined area in (**C**) showed the structure of long OS (**D**, arrow). (**E, F**) Grafted iNPCs were visualized by STEM121 peroxidase antibody (dark staining). Shed OS (arrows) were observed within the cytoplasm of grafted-iNPCs (asterisks). INL: inner nuclear layer; ONL: outer nuclear layer; IS: inner segment; OS: outer segment; DZ: debris zone. Scale bars: 50 μm (A, B), 2 μm (C, D), 500nm (E, F).

Author Manuscript

Author Manuscript

Author Manuscript

Author Manuscript

Table 1

PCR primer sequences, amplicon size, and melting temperature

mRNA	Forward primer (5′-3′)	Reverse primer (5′-3′)	Tm (°C)	Amplicon size (bp)
Itgav	CCTGTGCCTGTGTGGGTGAT	GGTGGCCGGACCCGTTTA	58	110
Itgb5	CGAGCGTGGGCACTGTCTCT	GCAGGCACTCGACGCAATCT	62	128
Ctsd	AGCTGGGAGGCAAAGGCTAC	CCCTGTTGTTGTCACGGTCA	58	188
Clta	AGAGCCACCCTGTGGAAACA	GCTTCCCTCCCCTTCCTCTT	55.5	215
Fak	ATGTGACGGGCCTGGTGAAAGG	TGGGTGCTGGCTGGTAGGAG	60	160
Mertk	GTGAGGCAGCGTGCATGAAAG	GGGCTTTGGGATGCCTTGAG	58	95
Tbp	GAACCACGGCACTGATTTC	CCCCACCATATTCTGAATCT	53	157